

# Effect Of Reaction Parameters On The Material Properties Of Highly Crystalline Anatase Titania Nanopowders

Sheeba Anu Jacob

S. Jerome Das

Department of Physics, Loyola College,  
Chennai, India

**Abstract:** *In the present work anatase Titania nanopowders were synthesized through solvothermal technique. The prime focus of the work has been to produce highly crystalline, polydisperse and roughly spherical TiO<sub>2</sub> nanoparticles with good surface area by controlling two important parameters namely reaction time and reaction temperature. The structural characterization done using XRD and FTIR reveals a tetragonal structure with enhanced crystallinity and the presence of appropriate functional groups for the synthesized anatase Titanium dioxide nanoparticles. The synthesized nanoparticles exhibit a high surface area. Extensive studies on the optical properties were done using UV-vis spectroscopy and Photoluminescence spectroscopy show the absorption edge to be red-shifted. The band gap values were evaluated using the Kubelka - Munk function and the direct band gap values were found to be approximately  $3.0 \pm 0.05$  eV for all the samples. The recorded emission spectrum was found to be of good optical quality with bands pertinent to the synthesized material. The HR-TEM images of the synthesized material exhibit a spherical nature and the SAED patterns display high degree of crystallinity.*

**Keywords:** *solvothermal synthesis, highly crystalline, high surface area, direct band gap*

## I. INTRODUCTION

Titanium dioxide is a promising nanomaterial that has made remarkable progress and finds extensive applications in photochromic devices [1] catalyst [2], solar cells [3], sensors[4], photovoltaics [5], and photocatalysis [6]. The anatase phase of the material with its high-potential properties like wide band gap (3.2 eV), strong oxidizing power, maximum light scattering, efficient light transportation and enhanced surface area modifications finds wide-spread applications. The properties of anatase Titanium dioxide have been studied extensively and are synthesized through several methods like sol-gel, solvothermal, hydrothermal, micelle and inverse micelle usage, direct oxidation, electro deposition, hydrolysis precipitation, ultrasonic and microwave methods [6-8]. However, it has been substantially proved that the performance of nanostructured TiO<sub>2</sub> particles are highly dependent on its material properties like crystalline structure, particle size morphology, phase purity, solubility, dimensions

etc. [6-8]. The solvothermal synthesis of these materials needs a proper optimization of its reaction time and temperature for appropriate utility of the material for extended applications. Templates or surfactants have been used in many a synthesis to produce the desired morphology and these have been experimented with various solvents to produce the desired morphology [9].

In our present work, we have used a template free solvothermal synthesis with a bulky precursor Titanium (IV) Butoxide, which allows for slow condensation. This bulky precursor has been widely reported only in the synthesis of mesoporous spheres, microspheres, nanospheres, hollow spheres etc. Studies hardly report the use of this precursor in a template free solvothermal synthesis by controlling the reaction parameters to produce highly crystalline nanoparticles with good surface area. Thus, striking a balance between high specific surface area and crystallinity will improve the utility of the material in photocatalytic activity and solar cell applications.

## II. MATERIALS AND METHOD

Tetrabutylorthotitanate  $[Ti(OBu)^4]$  purchased from Merck was used as the Titanium source. The solvent used was absolute ethanol. The precursor and the solvent were used without any further purification.

The precursor and solvent was mixed with a molar ratio of 1:3. The turbid solution was then subjected to magnetic stirring for few hours at ambient temperature to make a clear and homogenous solution. The pH of the solution was maintained at 5. It was then transferred into a 150 ml stainless steel Teflon-lined autoclave and maintained at temperatures 150 and 220 °C for two different reaction timings of 13 and 16 h respectively to analyze the influence of these parameters on the final product. The autoclave was cooled to room temperature and the sol thus obtained was washed several times by centrifuging with ethanol and double distilled water alternately and then filtered. The product thus obtained was dried in an oven at 70 °C for 24 h. The dried powders were ground well in a ceramic mortar and sintered at 400 °C for 4 h in a furnace.

## III. RESULTS AND DISCUSSIONS

### A. STRUCTURAL CHARACTERIZATION

The X-ray diffraction patterns were recorded using Sumens D5000 instrument with Cu  $K\alpha$  radiation ( $\lambda=1.540598 \text{ \AA}$ ) in the  $2\theta$  range 10 - 70° to identify the phase formation and to calculate the crystallite size using Scherrer's formula [10]. The X-ray diffraction patterns for as-synthesized  $TiO_2$  samples and heat-treated  $TiO_2$  samples at 150 and 220 °C for 13 and 16 h respectively are shown in Fig. 1 (A) and (B). The samples display a tetragonal crystal structure and the diffraction peaks indexed as (101), (004), (200), (105), (211) and (204) correspond to Anatase  $TiO_2$  (JCPDS, 83-2243). A small peak at 30.7° corresponding to the Brookite phase of  $TiO_2$  is visible in all the samples [11].

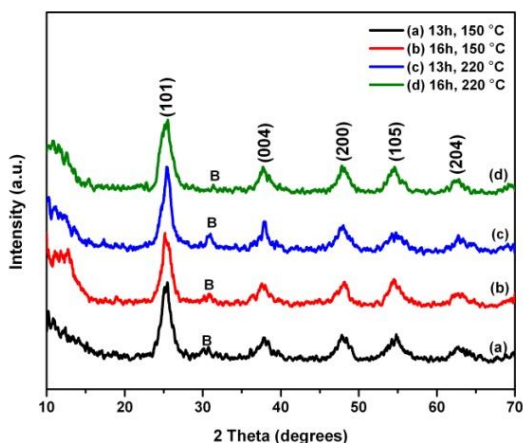


Figure 1 (A): XRD patterns for as-synthesized  $TiO_2$  nanoparticles (a) 13h, 150 °C, (b) 16h, 150 °C, (c) 13h, 220 °C, (d) 16h, 220 °C

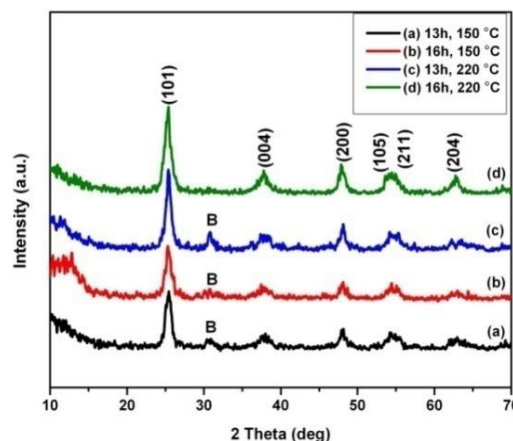


Figure 1 (B): XRD patterns for  $TiO_2$  nanoparticles heat-treated at 400 °C (a) 13h, 150 °C, (b) 16h, 150 °C, (c) 13h, 220 °C, (d) 16h, 220 °C

The crystallite size calculated using Scherrer's formula for the most prominent peak (101) is shown in Table 2. A quantitative evaluation of the crystallinity for the most prominent diffraction peak reveals an average crystallite size of ~7 nm for as-synthesized and ~11 nm for heat-treated samples respectively. The increase in the crystallite size can be attributed to the enhanced crystallinity after heat-treatment. It can be observed that with an increase in the reaction temperature, the phase formation is predominantly enhanced with a narrowing effect on the peak width, thus revealing the formation of greater  $TiO_2$  nanocrystallites. Correspondingly, an increase in the reaction time displays an increase in the peak intensities underlining the fact that longer hydrothermal time promotes growth of  $TiO_2$  nanocrystallites through Ostwald ripening [12]. It can be seen from Fig. 1 (B) that the  $TiO_2$  samples that are heat-treated at 400 °C display intense peaks and good crystallinity. Further, it can also be seen that among the four samples, the sample (c) is highly crystalline and sample (d) displays the highest phase purity.

The micro strain and micro stress values for the synthesized samples for three prominent peak positions (101), (200) and (105) are calculated and displayed in Table 1. It can be observed that there is a narrow shift in the d-spacing values with respect to the standard JCPDS d-spacing values, which indicates a micro strain present in the sample. Further since  $d_o < d_s$ , the calculated micro strain is negative. This indicates the generation of a residual compressive stress on the surface of the samples. From the micro strain values, the micro stress present in the sample was also calculated using the Young's Modulus value of the material.

| Temp. (°C) | Peak position (2θ) (deg) | hkl   | Inter planar distance $d_{hkl}$ (Å) |                    | Deviation in $d_{hkl}$ | Microstrain E | Microstress $\sigma_{stress}$ |
|------------|--------------------------|-------|-------------------------------------|--------------------|------------------------|---------------|-------------------------------|
|            |                          |       | observed ( $d_o$ )                  | standard ( $d_s$ ) |                        |               |                               |
| 150        | 25.376                   | (101) | 3.5070                              | 3.5126             | -0.0056                | -0.0015942    | -0.225387                     |
| 150        | 48.149                   | (200) | 1.8883                              | 1.8900             | -0.0017                | -0.0008994    | -0.127157                     |
| 150        | 54.219                   | (105) | 1.6897                              | 1.6990             | -0.0093                | -0.0054738    | -0.773885                     |
| 220        | 25.439                   | (101) | 3.4985                              | 3.5126             | -0.0141                | -0.0040141    | -0.567513                     |
| 220        | 48.135                   | (200) | 1.8888                              | 1.8900             | -0.0012                | -0.0006349    | -0.089762                     |
| 220        | 54.205                   | (105) | 1.6908                              | 1.6900             | -0.0082                | -0.0048263    | -0.682342                     |

Table 1: Line shifting and calculated micro strain and micro stress for three prominent peak positions

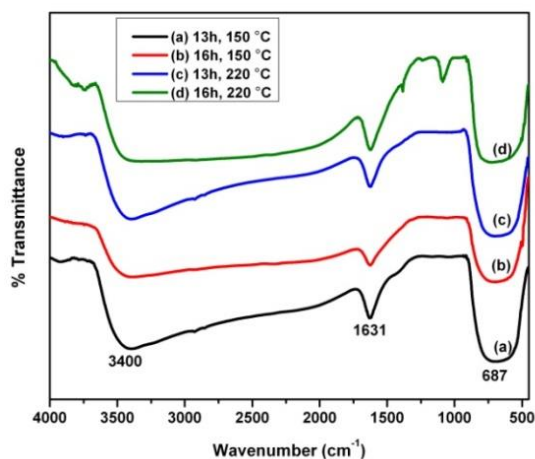


Figure 2: (a) 13h, 150 °C, (b) 16h, 150 °C, (c) 13h, 220 °C, (d) 16h, 220 °C

Fig. 2 shows the FTIR spectrum recorded using Perkin Elmer spectrometer by KBr pellet technique in the range of 4000 - 400  $\text{cm}^{-1}$  for the heat-treated  $\text{TiO}_2$  samples. The broad band centered around 3400  $\text{cm}^{-1}$  corresponds to the asymmetric and symmetric stretching vibrations of surface-adsorbed hydroxyl groups. These bands have decreased intensities and appear shallow. The relatively sharp band at 1631  $\text{cm}^{-1}$  can be attributed to the H-O-H bending modes of water molecules. The presence of a flat absorption band with enhanced intensity in the range of 800  $\text{cm}^{-1}$  - 600  $\text{cm}^{-1}$  indicates the contributions from Ti-O-Ti vibrations of anatase phase of titania. Further, the two peaks that appear in sample (d) at 1388 and 1088  $\text{cm}^{-1}$  correspond to the bending vibrations of C-H group and the characteristic vibrations of Ti-O-C group respectively.

## B. MORPHOLOGICAL CHARACTERIZATION

Fig.4A and 4B shows the HR-TEM images recorded using FEI-TECHNAI, G2-Model T30 High Resolution Transmission Electron microscope (HRTEM) at an accelerating voltage of 250 kV at two different magnifications for heat-treated  $\text{TiO}_2$  samples synthesized at 150 °C for 13h and Fig. 4C and 4D for samples synthesized at 220 °C for 16h. The images display numerous primary  $\text{TiO}_2$  particles in the form of roughly spherical spheres with crystallite sizes in the range of 10 - 15 nm, which is in good agreement with the XRD results whereas the heat-treated  $\text{TiO}_2$  samples display an average particle size of 11 nm. An increase in temperature to 220 °C causes the particles to attain good uniformity and better crystallinity, which is vividly seen through the SAED patterns. The phase evolution due to thermal annealing can be understood by the arrangement of the diffracted rings. The SAED ring pattern shown in the inset of Fig. 4C reflects the highly crystalline nature of the sample synthesized at 220 °C as compared to the sample at 150 °C. The d-spacings obtained from the XRD results are in good conformation with SAED pattern rings and hence are indexed in Fig. 4C. The morphological presentation reinstates and adds to the results obtained from the other studies.

The compositional conformation for the synthesized material was performed using EDX and the peaks

corresponding to Ti and O were found to be present in appropriate values as shown in Fig. 3A and 3B. The atomic percentage composition of the elements present are Ti=26.89% and O=73.11% for sample synthesized at 13h and 150 °C and Ti=20.30% and O=79.70% for sample synthesized at 16h and 220 °C respectively. It can be clearly inferred from the above details that the increase in reaction time (13h to 16h) and reaction temperature (150 °C to 220 °C) has resulted in the increase of oxygen vacancies in the sample as reported by M. Jaculine et.al [13].

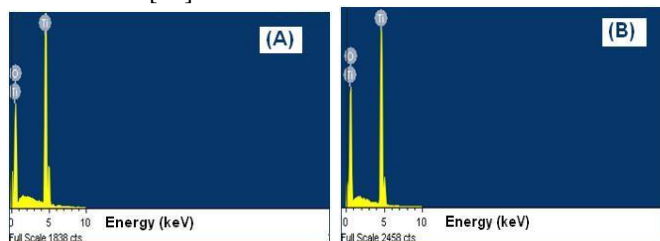


Figure 3: EDX spectra for heat-treated  $\text{TiO}_2$  nanoparticles at (A) 13h 150 °C, (B) 16h 220 °C

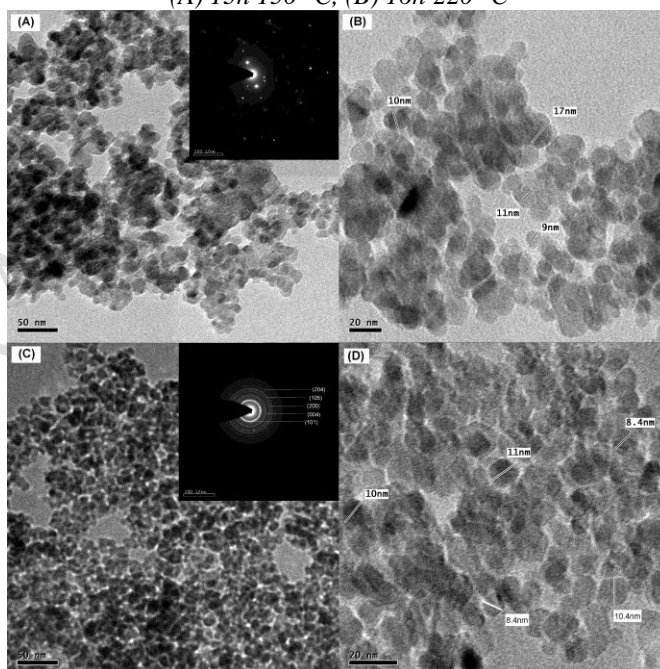


Figure 4: HR-TEM images for heat-treated  $\text{TiO}_2$  nanoparticles (A), (B) for 13h 150 °C and (C), (D) for 16h 220 °C

## C. SURFACE CHARACTERIZATION

The Multipoint BET Surface area measurements were done on a Quantachrome NovaWin - Data Acquisition and Reduction Instrument after degassing the samples in Nitrogen atmosphere at 300 °C for 1 hour with a bath temperature of 77.35 K. The BET surface area, total pore volume and the average pore size is given in Table 2. With increasing hydrothermal reaction temperature, it can be seen that the average pore size increases, indicating the growth of pores. This can be attributed to the enhancement in crystallization and the growth of anatase nanocrystallites [14]. With increasing hydrothermal reaction time, it can be seen that the average pore size increases. This can be due to the increase in crystallite sizes of the  $\text{TiO}_2$  powders. Simultaneously, there is

a monotonic decrease in pore volumes and BET surface areas, which could be due to the disappearance of small pores [11,14]. A higher surface area is revealed at 150 °C, which undergoes grain growth through Ostwald-ripening to form individual nano crystallites at 220 °C with a lesser surface area. A higher pore volume at 150 °C as compared to 220 °C agrees with the above statement [15]. A deviation from the above discussion is seen in the case of sample (d), with a decrease in average pore size, crystallite size and an increase in BET surface area. This could possibly be due to the change in crystallite size, which could alter the size and distribution of the inter-particle pores.

| Time (h) | Temperature (°C) | Particle size (nm) | Bandgap $E_g$ (eV) |          | $S_{BET}$ (m <sup>2</sup> /g) | Total pore volume (cc/g) | Average pore size (Å) |
|----------|------------------|--------------------|--------------------|----------|-------------------------------|--------------------------|-----------------------|
|          |                  |                    | Direct             | Indirect |                               |                          |                       |
| 13       | 150              | 8.43               | 2.99               | 2.43     | 120.545                       | 0.04984                  | 8.270                 |
| 13       | 220              | 13.3               | 2.95               | 2.32     | 113.712                       | 0.04732                  | 8.322                 |
| 16       | 150              | 11.8               | 3.03               | 2.73     | 93.062                        | 0.04871                  | 8.319                 |
| 16       | 220              | 8.16               | 3.00               | 2.55     | 109.140                       | 0.04459                  | 8.170                 |

Table 2: Physicochemical parameters for TiO<sub>2</sub> nanoparticles and the calculated particle size for the most prominent peak at (101)

#### D. OPTICAL CHARACTERIZATION

##### UV-VIS AND PL SPECTROSCOPY

The spectroscopic properties were recorded on Specord S600 – 212C205 in the wavelength range of 390 – 800 nm. The absorption edge in Fig. 5A is found to be centered around 425 nm for all the samples, beyond which the samples are completely transparent. The absorption edge is prominently red-shifted, which indicates a decrease in the band gap. This could be due to the difference in the surface microstructure, composition and phase structure in the TiO<sub>2</sub> powder.

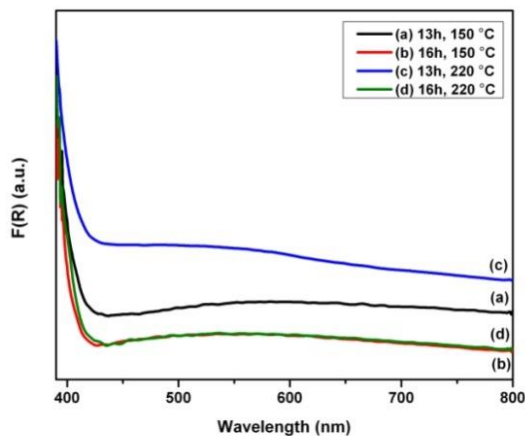


Figure 5 A: Absorbance plots for TiO<sub>2</sub> nanoparticles synthesized for (a) 13h 150 °C (b) 16h 150 °C (c) 13h 220 °C (d) 16h 220 °C

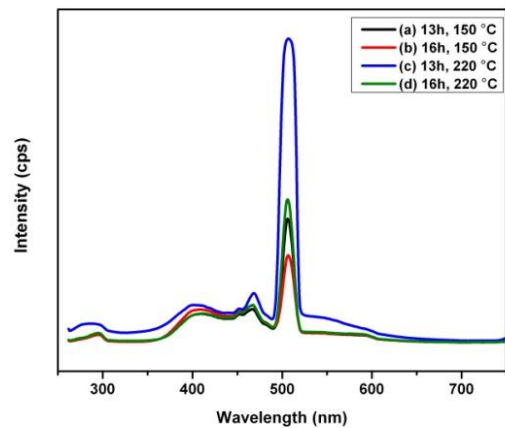


Figure 5 B: PL spectra for TiO<sub>2</sub> nanoparticles synthesized for (a) 13h 150 °C (b) 16h 150 °C (c) 13h 220 °C (d) 16h 220 °C

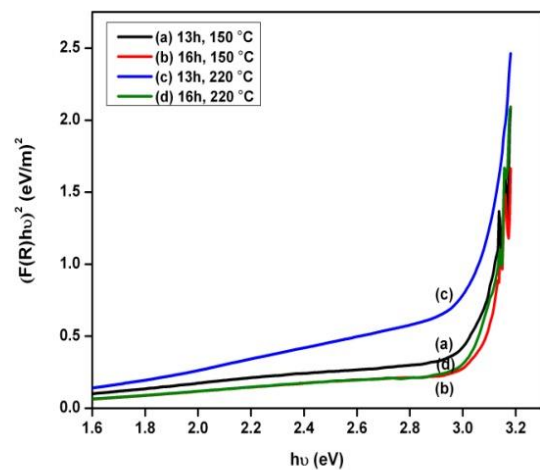


Figure 5 C: Kubelka – Munk plot for direct transitions in TiO<sub>2</sub> nanoparticles at (a) 13h 150 °C (b) 16h 150 °C (c) 13h 220 °C (d) 16h 220 °C

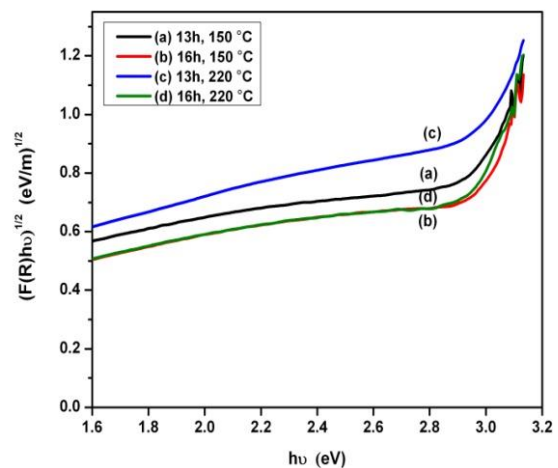


Figure 5 D: Kubelka – Munk plot for indirect transitions in TiO<sub>2</sub> nanoparticles at (a) 13h 150 °C (b) 16h 150 °C (c) 13h 220 °C (d) 16h 220 °C

The re-emission function of Kubelka-Munk [16] was used to determine the band gaps of the synthesized samples. A plot of the Kubelka - Munk function for both direct and indirect transitions for the synthesized samples is shown in Fig.5C and 5D. The optical values of band gap were determined by extrapolating the linear part of the graph to the axis of the abscissa. From the band gap values tabulated in Table 2, it can be seen that the indirect optical band gaps for anatase TiO<sub>2</sub> is  $\sim 2.5 \pm 0.2$  eV, which is quite unrealistic. The direct optical band gap was found to be  $\sim 3.0 \pm 0.05$  eV for direct transitions which is close to the reported value of 3.2 eV for anatase TiO<sub>2</sub>. This is in line with the work of Reddy et al., [17] which reports a low value of E<sub>g</sub> for indirect transitions and favours direct transitions for anatase TiO<sub>2</sub> nanoparticles. The minor variations in the direct band gap values for anatase TiO<sub>2</sub> nanoparticles can be attributed to variations in the stoichiometry during synthesis, the impurity content and the crystalline size [18]. It can be further observed that although variations in temperature does not affect the band gap significantly, minor variations in time leads to a change in the band gap value by  $\sim 0.1$  eV, which could be possibly due to the particle size variations as discussed earlier.

Fig.5B shows the room temperature PL emission spectra recorded on a JOBIN YVON FLUOROLOG-3-11 SPECTROFLUORIMETER with a 450W Xenon Lamp as source for the synthesized samples at an excitation wavelength of 252 nm. The spectrum for all the samples show three emission bands. The flat band centered around 402 nm corresponds to the excitonic PL peaks trapped by surface states and defects and hence is easily affected by factors related to surface. The two sharp peaks centered approximately at 467 nm and 506 nm within the band region of 450 - 520 nm is attributed to the oxygen defect trapped excitonic PL peak [19]. However for all the samples, the peak at 506 nm expresses itself prominently with high intensity. Among the four samples, sample (c) displays the highest intensity. This can be endorsed to the high degree of crystallinity exhibited by this sample, as is evident from the XRD results. Further as discussed by Amita et al., [20], the least transparent films exhibit the highest PL intensity. Thus it is evident that the sample (c) and (d) synthesized at 220 °C for different reaction time exhibits the least transparency as compared to sample (a) and (b) synthesized at 150 °C which exhibit high transparency.

#### IV. CONCLUSIONS

The prime focus of the present work has been to synthesize highly crystalline anatase TiO<sub>2</sub> nanoparticles with focus on reaction time and reaction temperature using a simple solvothermal technique. The enhanced crystallinity and grain growth seen in the samples are concluded to be direct results of influence of reaction time and temperature. This is further validated with the high surface area exhibited by the samples and an increase in average pore size indicating the growth of pores. Further, the micro strain values indicates the generation of a residual compressive stress on the surface of the samples. The morphological appearance of the samples further testify that the reaction time and temperature not only influences the

grain growth but also their aggregating behaviour. With a decrease in the direct band gap value and good transparency in the visible region, the optical properties attach further importance to the work. With light to the above discussions, we may therefore conclude that in the present work, the most optimum condition for the synthesis of TiO<sub>2</sub> nanoparticles is at 150 °C for 13 h. Their excellent properties show promising applications in Dye-sensitized solar cells.

#### ACKNOWLEDGEMENT

The authors (Sheeba Anu Jacob & S. Jerome Das) gratefully acknowledge the financial assistance from Department of Science and Technology (DST), Government of India through the project [REF: SR/WOS-A/PS-16/2012 (G)] under Women Scientist Scheme (WOS-A).

The author records her thanks to the various Instrumentation facilities extended by SAIF, IIT-M, SATF, IISc., Bangalore, Department of Nuclear Physics, Madras University and NCNSNT, Madras University.

#### REFERENCES

- [1] Fujishima, K. Honda, Electrochemical Photolysis of water at a Semiconductor electrode, *Nature* 238 (1972) 37 – 38.
- [2] S. K. Maity, M. S. Rana, S. K. Bej, J. Ancheyta-Juarez, G. M. Dhar, T. S. R. P. Rao, TiO<sub>2</sub> - ZrO<sub>2</sub> mixed oxide as a support for hydro treating catalyst, *Catal. Letters* 72 (2001) 115 - 119.
- [3] G. K. Mor, K. Shankar, M. Paulose, O. K. Varghese, C. A. Grimes, Use of highly-ordered TiO(2) nanotube arrays in dye-sensitized solar cells, *Nano Lett.* 6 (2006) 215 - 218.
- [4] C. Garzella, E. Comini, E. Tempesti, C. Frigeri, G. Sberveglieri, TiO<sub>2</sub> thin films by a novel sol-gel processing for gas sensor applications. *Sens. Actuators, B* 68 (2000) 189 - 196.
- [5] A. C. Fisher, L. M. Peter, E. A. Ponomarev, A.B. Walker, K.G.U. Wijayantha, Intensity Dependence of the back reaction and transport of electrons in dye-sensitized Nanocrystalline TiO<sub>2</sub> solar cells, *J. Phys. Chem. B* 104 (2000) 949 – 958.
- [6] X. Chen, S.S. Mao, Titanium dioxide nanomaterials: synthesis, properties, modifications and applications, *Chem. Rev.* 107 (2007) 2891 - 2959.
- [7] C. Burda, X. Chen, R. Narayanan, M.A. El-Sayed, Chemistry and properties of nanocrystals of different shapes, *Chem. Rev.* 105 (2005) 1025 – 1102.
- [8] L. T. Mancic, B. A. Marinkovic, P. M. Jardim, O. B. Milosevic, F. Rizzo, Precursor particle size as the key parameter for Isothermal tuning of morphology from nanofibers to nanotubes in the Na<sub>2</sub>-xHxTinO<sub>2n+1</sub> system through Hydrothermal alkali treatment of Rutile mineral sand, *Cryst. Growth Des.* 9 (2009) 2152 – 2158.
- [9] R. A. Roca, E. R. Leite, Size and shape tailoring of Titania nanoparticles synthesized by solvothermal route in different solvents, *J. Am. Ceram. Soc.*, 96, 1(2013) 96 - 102.

- [10] J. C. Yu, L. Z. Zhang, J. G. Yu, Direct sonochemical preparation and characterization of highly active mesoporous TiO<sub>2</sub> with a bicrystalline framework, *Chem. Mater.* 14 (2002) 4647-4653.
- [11] E. P. Melian, O.G. Diaz, J.M.D. Rodriguez, G. Colon, J.A. Navio, J. Perez pena, Effect of hydrothermal treatment on the structural and photocatalytic properties of TiO<sub>2</sub> synthesized by sol-gel method, *Applied Catalysis A: General* 411-412 (2012) 153-159.
- [12] R. Boistelle, J.P. Astier, Crystallization mechanisms in solutions, *J. Cryst. Growth* 90 (1988) 14.
- [13] M. Jaculine, C. Justin Raj, S. Jerome Das, Hydrothermal synthesis of highly crystalline Zn<sub>2</sub>SnO<sub>4</sub> nanoparticles and their optical properties, *J. Alloys and Compounds* 577 (2013) 131 - 137
- [14] J. Yu, G. Wang, B. Cheng, M. Zhou, Effects of hydrothermal temperature and time on the photocatalytic activity and microstructures of bimodal mesoporous TiO<sub>2</sub> powders, *Applied Catalysis B: Environmental* 69 (2007) 171 -180.
- [15] J. Yu, H. Yu, B. Cheng, M. Zhou, X. Zhao, Enhanced photocatalytic activity of TiO<sub>2</sub> powder (P25) by hydrothermal treatment, *J. Molecular Catalysis A: Chemical* 253 (2006) 112-118.
- [16] A. Furube, T. Asahi, H. Masuhara, H. Yamashita, M. Anpo, *J. Phys.Chem.B1* 03 (1999) 3120.
- [17] K. Reddy, S. Manorama, A. Reddy, Bandgap studies on anatase titanium dioxide nanoparticles, *Mater. Chem. Phys.* 78 (2002) 239-245.
- [18] F. Hossain, L. Sheppard, J. Nowotny, G. Murch, Optical properties of anatase and rutile titanium dioxide: Ab initio calculations for pure and anion-doped material, *J. Phys. Chem. Solids* 69 (2008) 1820 –1828.
- [19] L. Q. Jing, Y. C. Qu, B. Q. Wang, Review of photoluminescence performance of nano-sized semiconductor materials and its relationships with photocatalytic activity, *Sol. Energy mater. Sol. C* 90 (2006) 1773-1787.
- [20] A. Verma, A. G. Joshi, Structural, Optical, Photoluminescence and photocatalytic characteristics of sol-gel derived CeO<sub>2</sub>-TiO<sub>2</sub> films, *Indian J. Chem.* 48A (2009) 161-167.